Volumetric mix-design modification and vibration attenuation analysis of rubberised epoxy asphalt track for railway

Shi, Chenguang; Wu, You; Fuentes, Raul; Fan, Yulou; Zhou, Yixin; Fu, Chaoliang; Yang, Jun

DOI
10.1080/14680629.2024.2432569

Publication date
2024

Document Version
Final published version

Published in
Road Materials and Pavement Design

Citation (APA)
Shi, C., Wu, Y., Fuentes, R., Fan, Y., Zhou, Y., Fu, C., & Yang, J. (2024). Volumetric mix-design modification and vibration attenuation analysis of rubberised epoxy asphalt track for railway. *Road Materials and Pavement Design*, *26*(8), 1890-1913. https://doi.org/10.1080/14680629.2024.2432569

Road Materials and Pavement Design

ISSN: (Print) (Online) Journal homepage: www.tandfonline.com/journals/trmp20

Volumetric mix-design modification and vibration attenuation analysis of rubberised epoxy asphalt track for railway

Chenguang Shi, You Wu, Raul Fuentes, Yulou Fan, Yixin Zhou, Chaoliang Fu & Jun Yang

To cite this article: Chenguang Shi, You Wu, Raul Fuentes, Yulou Fan, Yixin Zhou, Chaoliang Fu & Jun Yang (02 Dec 2024): Volumetric mix-design modification and vibration attenuation analysis of rubberised epoxy asphalt track for railway, Road Materials and Pavement Design, DOI: 10.1080/14680629.2024.2432569

To link to this article: https://doi.org/10.1080/14680629.2024.2432569

ROAD MATERIALS AND PAVEMENT DESIGN
https://doi.org/10.1080/14680629.2024.2432569

Volumetric mix-design modification and vibration attenuation analysis of rubberised epoxy asphalt track for railway

Chenguang Shi[a,b,c,d], You Wu[e], Raul Fuentes[d], Yulou Fan[c], Yixin Zhou[c], Chaoliang Fu[f] and Jun Yang[c]

[a]National & Local Joint Engineering Research Center of Transportation and Civil Engineering Materials, Chongqing Jiaotong University, Chonqing, People's Republic of China; [b]School of Civil Engineering, Chongqing Jiaotong University, Chongqin, People's Republic of China; [c]School of Transportation, Southeast University, Nanjing, People's Republic of China; [d]Institute of Geomechanics and Underground Technology, RWTH Aachen University, Aachen, Germany; [e]Section of Railway Engineering, Delft University of Technology, Delft, the Netherlands; [f]Institute of Highway Engineering (ISAC), RWTH Aachen University, Aachen, Germany

ABSTRACT

Rubberized asphalt mixture effectively reduces vibrations in railway track due to the elasticity of crumb rubber (CR) and the viscoelasticity of asphalt binder. This study aims to design a rubberized epoxy asphalt mixture using the modified volumetric mix-design method named the multi-point supported skeleton for asphalt mixtures (V-S method). The feasibility and vibration attenuation of the precast epoxy asphalt track was evaluated through a 3D FEM simulation at a 350 km/h speed. By combining the V-S method with the equivalent volume replacement principle between CR and coarse aggregate, four types of rubberized epoxy asphalt mixtures were proposed using the dry method. Indoor test results confirm that these mixtures meet the required specifications. The FEM results demonstrate that the designed epoxy asphalt track meets the design criteria and the components of the EA-4CR track structure demonstrate superior vibration reduction performance among the cases with the same increment in CR content.

ARTICLE HISTORY
Received 3 July 2024
Accepted 15 November 2024

KEYWORDS
High-speed railway; bi-block precast epoxy asphalt track; volumetric mix-design; finite element method; dynamic response; vibration attenuation

1. Introduction

The trackbed is a vital component of railway track structures, providing support, damping vibrations, insulating noise, facilitating drainage, and protecting infrastructure. It serves multiple functions essential for ensuring safe, stable, and comfortable track operation. Currently, two main track structures are used in railway engineering: ballasted and ballastless track (Shi et al., 2022). However, the frequent maintenance required for ballasted tracks and the challenges in maintaining ballastless tracks present problems. To address these challenges, bituminous trackbeds are widely applied in railway structures due to the viscoelastic properties of asphalt materials, such as asphalt underlayment (AUL), asphalt overlayment (AOL), surface asphalt mixture impermeable (SAMI), and asphalt stabilised ballast (ASB) (Fang et al., 2019).

The current application of asphalt trackbeds primarily involves AOL in ballasted tracks as a sub-ballast layer (Alves et al., 2022; Castro et al., 2022; Di Mino & Di Liberto, 2012; Esmaeili et al., 2018; Khairallah et al., 2022; Liu et al., 2024) and in ballastless tracks as support for concrete slab tracks and for waterproofing purposes (Lee et al., 2021, 2023; Liu et al., 2018, 2019). Surface asphalt mixture

CONTACT Jun Yang yangjun@seu.edu.cn

impermeable (SAMI) is only paved on the subgrade shoulder of the crushed stone layer and in the middle of double lines for waterproof function, serving as a functional layer rather than a structural layer (Fang et al., 2017). Asphalt stabilised ballast (ASB) is used to maintain the geometry stability of ballast under repeated train loading (Bressi et al., 2018). There have been a few instances where ballastless tracks were constructed with asphalt layers as trackbeds, particularly AOL. The most well-known application of AOL is the GETRAC system, where concrete sleepers are directly placed on an asphalt layer. This system was proposed by Deutsche Bahn as a low-maintenance alternative to conventional ballasted tracks, aiming to preserve natural resources (Ramirez Cardona et al., 2020). Recently, several laboratory studies have emerged (Bose et al., 2020, 2021; Lee et al., 2023; Shi et al., 2021, 2022; Wang et al., 2022). These studies have explored various aspects of AOL, including Lee's work (2023) and Bose's research (2020, 2021), which involved directly placing sleepers on top of continuous asphalt pavement in their experiments. Geotextiles were attached to the bottom of sleepers to increase the frictional force between the sleepers and the asphalt layer. However, the test results of track stiffness and rail foundation modulus were relatively low due to the use of normal asphalt mixture (thermoplastic asphalt, such as matrix asphalt, polymer-modified asphalt, etc.) and inadequate bonding of the geotextile, which can lead to rapid degradation of the railway structure. These deficiencies in the railway structure, indicated by low track stiffness and rail foundation modulus, can negatively impact stability and performance. In previous studies (Shi et al., 2021, 2022; Wu et al., 2023), we proposed a new type of precast bi-block epoxy asphalt discontinuous trackbed structure, which demonstrates excellent strength of the epoxy asphalt binder and stronger bonding between the asphalt layer and sleepers. This precast bi-block asphalt trackbed unit, consisting of a sleeper and two precast asphalt blocks, is manufactured in the factory and transported to the construction site for unit construction and maintenance.

The design of asphalt mixtures for railway tracks is a critical consideration (Jadidi et al., 2021; Zhang et al., 2023). The material design of the asphalt layer in track structures is directly influenced by its geometric features and mechanical properties, which impose specific requirements (Fang et al., 2020). In both AOL and AUL systems, the asphalt layer must possess sufficient strength to withstand train loads while offering resistance to moisture and fatigue. In AOL, there is an added focus on vibration control and noise reduction, where the asphalt layer plays a crucial role. Thus, designing the asphalt layer for AOL involves additional attention to factors enhancing vibration damping properties and noise reduction. Engineers and researchers optimise the composition and properties of the asphalt mixture by selecting suitable aggregate types, gradations, and binder formulations. They may also incorporate special additives or modifiers, such as crumb rubber (CR), to enhance vibration damping properties (Di Mino & Di Liberto, 2012; Shi et al., 2022; Soto, 2018; Soto & Mino, 2018; Wang et al., 2022). However, there is currently no specific mix design exclusively tailored for asphalt mixtures used in railway tracks. Instead, the aggregate gradation design often adopts the dense-graded asphalt mixture commonly employed in asphalt pavement. Furthermore, many studies use fine CR as a modifier to improve the elastic properties of asphalt mixtures. However, incorporating fine CR may increase the asphalt binder content and weaken the improvement achieved with the same volume of coarse CR. Therefore, the characteristics of CR, including particle size and volume used as a modifier in asphalt mixtures, significantly impact the resulting asphalt binder content, overall enhancement of elastic properties, and selection of aggregate gradation method.

The gradation of aggregates is crucial in determining the properties of asphalt mixtures (Fang et al., 2019). Asphalt mixtures can be categorised into skeleton-void, suspension-dense, and skeleton-dense based on their compositions (Borges Miranda et al., 2021; Zheng et al., 2012). The skeleton-dense asphalt mixture exhibits the best comprehensive performance due to its stable stone-to-stone skeleton, which results in larger cohesive force and internal friction (Zhang et al., 2019). Therefore, for designing the rubberised epoxy asphalt mixture in this study, the skeleton-dense asphalt mixture was chosen. This selection aims to achieve a hybrid rigid-flexible skeleton structure of the rubberised epoxy asphalt mixture through the dry method, replacing the coarse aggregates with CR of the same size. Various methods can be used to construct the skeleton-dense asphalt mixture, including the Coarse

Aggregate Void-filling (CAVF) method (Yu et al., 2020), the volumetric design method based on the multipoint supported skeleton (V-S) method (Li, Shang, Liu, et al., 2019a, 2019b), and the Gradation-based framework (Lira et al., 2013). Among these methods, the V-S method determines the skeleton structure of coarse aggregates with a loose packing of two continuous sieve sizes. Consequently, the smaller coarse aggregates play a significant role in the skeleton structure. This provides an opportunity to replace as many of the smallest coarse aggregates with CR as possible, enhancing the elastic properties of the mixtures and achieving the regulation of elasticity and vibration attenuation in asphalt trackbeds.

The objective is to gain a better understanding of the design method for rubberised epoxy asphalt mixtures and the damping performance of epoxy asphalt trackbeds through finite element (FE) simulation. The paper is organised as follows. Firstly, it presents characterisation of track structure and materials design for rubberised epoxy asphalt trackbeds. Moving on, section 3 conducts a mechanical response analysis of the designed epoxy asphalt track using FE numerical simulation. This analysis evaluates the feasibility of the epoxy asphalt track from mechanical behaviour and performance perspectives, providing valuable insights into the structural response and integrity of the track design. Subsequently, section 4 focuses on investigating the vibration reduction effect of CR content for the rubberised asphalt track through time-domain and frequency-domain analysis of acceleration. Finally, the paper concludes by summarising the findings and overall conclusions drawn from the study.

2. Structure characterisation and materials design of rubberised epoxy asphalt trackbeds

2.1. Structure characterisation of rubberised epoxy asphalt trackbeds

The structure of the epoxy asphalt trackbed consists of a flat-shaped unit, comprising one sleeper and two prefabricated asphalt mixture blocks, facilitating easier construction and maintenance processes. The schematic of the precast epoxy asphalt track structure and for the formation process of epoxy asphalt curing blocks are shown in Figure 1. More detailed information about the bi-block precast asphalt track can be found in (Shi et al., 2021, 2022). In a traditional ballasted track structure, it is typically assumed that the wheel-rail forces under a single axle are distributed among five neighbouring sleepers, as shown in Figure 2. The specific distribution of load depends on factors such as the type and stiffness of the sleepers used in the trackbed structure. The maximum vertical contact stress between the sleeper and the trackbed can be calculated using the following Equation (1) (Bian et al., 2020, 2023):

$$\sigma_{\max} = \frac{\theta P_s(1+\alpha v)}{A_e} \tag{1}$$

where P_s represents the static axle load of the train; α is the dynamic impact coefficient; θ is the load sharing coefficient for intermediate sleepers, taken as 0.46 (Bian et al., 2023); v is the train speed in km/h; A_e is the effective contact area between the sleeper and the trackbed, taken as 0.7 m^2 based on the size of sleeper.

At a train speed of 350 km/h, the maximum vertical contact stress between the sleeper and the ballasted trackbed is 260.3 kPa, assuming a ballasted trackbed with a α value of 0.0038 (China, 2014). For a ballastless trackbed, the contact stress is 335 kPa. It is important to note that these calculated contact stresses are significantly lower than the tire-ground pressure used in roadway pavement design, which is 700 kPa.

2.2. Design criteria and requirements of mechanical response index for epoxy asphalt track

To ensure the long-term effectiveness and safety of the prefabricated epoxy asphalt track, design indicators based on the concept of cumulative damage include the tensile strain at the bottom of the asphalt layer and the vertical compressive stress on the subgrade surface.

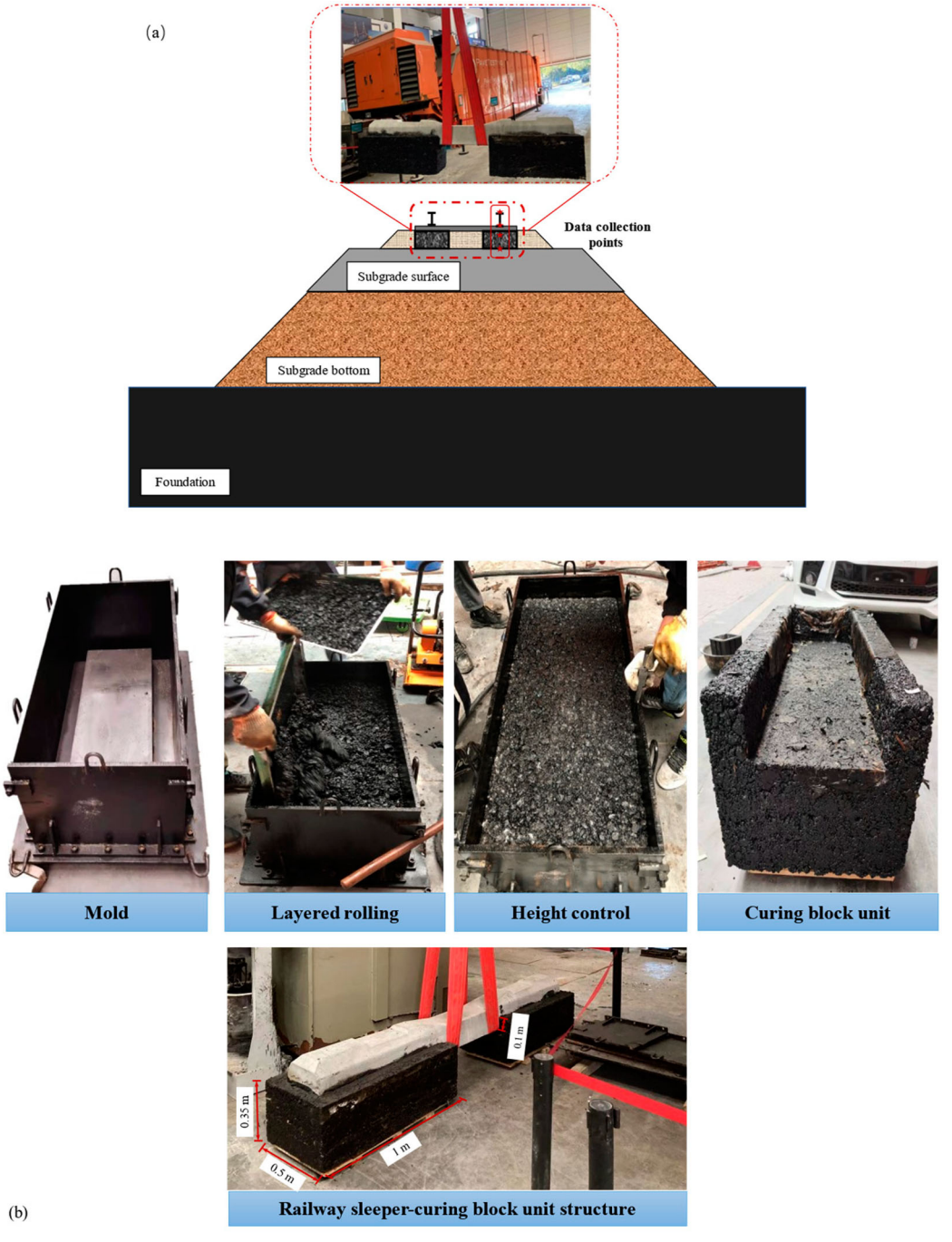

Figure 1. Structure characterisation includes (a) a transverse cross-sectional schematic diagram of the precast epoxy asphalt track and (b) the process of moulding railway sleepers with epoxy asphalt curing blocks.

Asphalt mixtures exhibit a progressive mechanical behaviour consisting of three stages: linear viscoelasticity, nonlinear viscoelasticity, and the damage stage, as strain levels increase (Luo et al., 2016). To prevent fatigue failure, the strain level in the asphalt mixture must remain below the fatigue endurance limit strain (Prowell et al., 2010). In fatigue tests, Ref. (Jin, 2017) obtained limit strains of

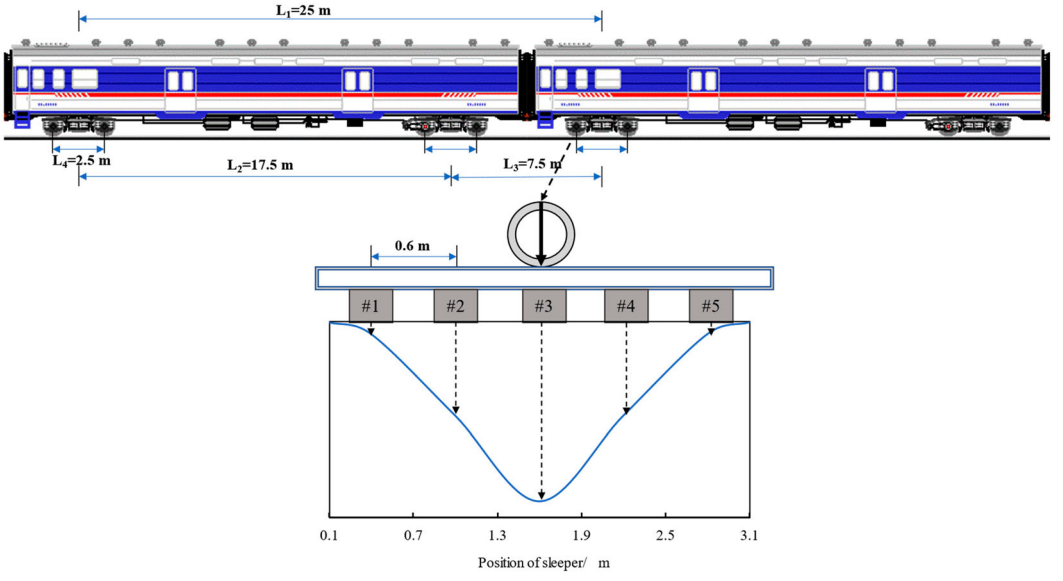

Figure 2. The single-axle load distribution on sleepers 1–5 when the wheel axle is directly above sleeper 3.

330 $\mu\varepsilon$ for epoxy asphalt mixture, 150 $\mu\varepsilon$ for SBS modified asphalt mixture, and 70 $\mu\varepsilon$ for normal asphalt mixture. In this study, FE numerical simulations are employed to determine the transverse and longitudinal tensile strains at the bottom of the curing blocks under train loading. As long as these strains remain below 330 $\mu\varepsilon$, it can be concluded that the designed epoxy asphalt track will not experience fatigue cracking.

Regarding the vertical compressive stress on the top of the subgrade surface, after the spreading effect of vehicle loads on the trackbed, they are transmitted to the subgrade surface from the upper structure. Controlling the vertical compressive stress on the subgrade surface effectively manages the subgrade deformation, ensuring a longitudinally uniform, stable, and smooth track structure. According to technical specification TB10761-2013 (China, 2013), the allowable values for dynamic loads on ballasted and ballastless track subgrades are 68 and 32.4 kPa, respectively. The precast epoxy asphalt track combines elements of both ballasted and ballastless trackbeds, aiming to provide enhanced performance and durability for railway systems. Therefore, the vertical compressive stress on the top of the subgrade surface should fall within the range of 32.4–68 kPa.

The performance evaluation involves assessing rail foundation modulus, track stiffness, acceleration in each structural layer, and vertical displacement of the subgrade surface. Rail foundation modulus and track stiffness are used to evaluate the track structure's vertical stability. Higher rail foundation modulus and track stiffness values indicate better load-bearing capacity and reduced vertical deflections, ensuring the track remains stable under varying loads. Dynamic performance evaluation focuses on managing acceleration in each structural layer. This control is crucial to preserve the track's integrity and prevent damage. Excessive vibration acceleration can lead to frictional damage, particle breakage, and plastic deformation. By monitoring and controlling acceleration, premature wear and potential failures can be avoided. Minimising vertical dynamic deformation ensures a high level of smoothness and stability, enhancing passenger safety and comfort. Monitoring and optimising these indicators enable railway authorities and engineers to ensure the track's long-term performance, durability, and passenger safety. The technical specification TB10761-2013 (China, 2013) provides regulations for acceleration on the top of rail, sleeper, and trackbed, as well as vertical displacement of the subgrade surface. These regulations are outlined in Table 1.

Table 1. Evaluation criteria for track structure dynamic performance (China, 2013).

Parameters	Ballastless track	Ballasted track
Acceleration on the top of rail (m/s^2)	5000	3000
Acceleration on the top of sleeper (m/s^2)	–	500
Acceleration on the top of trackbed (m/s^2)	300	–

2.3. Volumetric mix-design based on V-S method

This study employed V-S method for volumetric mix-design of epoxy asphalt mixture (Li, Shang, Liu, et al., 2019a, 2019b). This arrangement increases aggregate contact points, reducing contact stress and enhancing the load-carrying capacity of the skeleton system. In the V-S method, the boundary between coarse and fine aggregate sizes is set at 4.75 mm. Previous studies have shown that aggregates with a particle size of 4.75 mm are crucial for the skeleton structure, providing essential support to the larger-sized particles and significantly enhancing the load-bearing capacity of the asphalt mixture (Li, Shang, Pan, et al., 2019b). Coarse aggregates with a particle size of 4.75 mm or larger interlock to form the skeleton structure, while the remaining fine aggregates, fillers, and asphalt binder form the asphalt mastic, filling the voids within the skeleton structure. The design process of the V-S method consists of three parts, which include:

1. Gradation design of coarse aggregates for constructing a multi-point support skeleton structure

According to particle packing theory, the stress at contact points between particles in a single-size skeleton structure is proportional to the square of the particle size and the average stress across the entire skeleton structure. The V-S method design aims to increase the number of contact points by introducing a finer size fraction of aggregates, thereby reducing stress at the contact points. The multi-point support skeleton model, which incorporates coarse aggregates, is depicted in Figure 3. The volumetric ratio between adjacent size fractions is established using a two-dimensional unit represented by a three-dimensional cube within the dashed line range in the figure. The side length of the three-dimensional cube is ($d_i + d_{i+1}$). It consists of one large-sized particle (d_i) surrounded by numerous smaller-sized particles (d_{i+1}). The volume filling ratio (V_i) of particles in the unit is calculated using Equation (2). If the three-dimensional cube contains only one larger particle, its volume filling ratio ($V_{i,0}$) in the unit space is calculated using Equation (3). Dividing the two equations yields the volume-filling ratio of the coarser size fraction of aggregates in the model, as shown in Equation (4), where V_0 is the volume-filling ratio when the largest-sized (first fraction) particle is filled individually, and is the ratio of packing density to apparent density (Li, Shang, Liu, et al., 2019a, 2019b).

$$V_i = \frac{\frac{\pi d_i^3}{6}}{(d_i + d_{i+1})^3} \times 100 \tag{2}$$

$$V_{i,0} = \frac{\frac{\pi d_i^3}{6}}{d_i^3} \times 100 \tag{3}$$

$$V_i = \frac{V_0}{\left(1 + \frac{d_{i+1}}{d_i}\right)^3} \times 100 \tag{4}$$

Based on Equations (2)–(4), the volume percentages occupied by the first and second size fractions of aggregates can be determined. To calculate the volume fraction of a specific grade of coarse aggregates, the volume fractions of the larger coarse aggregates need to be subtracted. Similarly, the volume percentages of other size fractions of aggregates can be calculated using the same model and

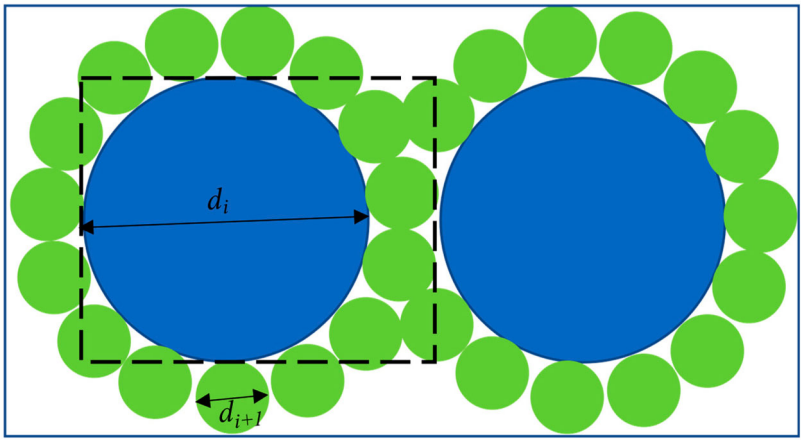

Figure 3. Design model of coarse aggregate skeleton and cubic element.

Equation (5).

$$\begin{cases} V_i^F = 100 - \sum_{j=1}^{i-1} V_j \\ V_i = \dfrac{V_0}{\left(1 + \frac{d_{i+1}}{d_i}\right)^3} V_i^F \times 100 \end{cases} \tag{5}$$

where V_i^F is the volume fraction (%) to be filled for the i grade of coarse aggregates, and V_i^F equals 100%.

2. Gradation design of fine aggregates (including fillers) used to fill the voids in the skeleton structure

Research findings suggest that aggregates with a particle size of 2.36 mm can destabilise the skeleton structure (Li, Shang, Pan, et al., 2019b). Hence, the fine aggregates used in this study have a particle size smaller than 2.36 mm, resulting in a discontinuous gradation. It is important to note that the gradation of fine aggregates, which is another component of the skeleton-fill system of the asphalt mixture, can be effectively designed using the theory of maximum density filling (as shown in Equation (6)):

$$P_k = \left(\frac{d_k}{D}\right)^{0.45} \times 100\% \tag{6}$$

where P_k is the percentage passing of sieve size d_k, D is the maximum particle size of fine aggregates, which is equal to 2.36 mm, herein. In the traditional maximum density theory, the exponent value usually ranges from 0.35 to 0.45. However, in the V-S design method, a recommended value of 0.25 is used to enhance the strength of the asphalt mastic by increasing the powder-to-binder ratio. In this particular study, a high-strength epoxy asphalt binder is utilised, and therefore, a value of 0.45 is employed.

3. Asphalt mixture proportion

Once the gradation design of coarse and fine aggregates is finalised, the next step is to calculate the required dosage of asphalt binder to achieve the desired overall proportion of the asphalt mixture. The asphalt binder enhances adhesion between the aggregates, improving the strength and

durability of the asphalt mixture. During the gradation design process, VCA and VMA are considered as control parameters, and the spatial volume filling relationships between coarse aggregates, fine aggregates, and asphalt binder are established using Equations (7)–(9). With the theoretical quantities of coarse and fine aggregates calculated in the previous steps, the gradation of the asphalt mixture can be determined (Li, Shang, Liu, et al., 2019a, 2019b).

$$P_c + P_f = 100 \tag{7}$$

$$\frac{P_f}{\rho_f} = \frac{P_c}{\rho_{cs}}\left(\frac{\mathrm{VCA} - \mathrm{VMA}}{100}\right) \tag{8}$$

$$\frac{P_a}{\rho_a} = \frac{P_c}{\rho_{cs}}\left(\frac{\mathrm{VMA} - \mathrm{VV}}{100}\right) \tag{9}$$

where P_c is the mass percentage of coarse aggregates, %. P_f is the mass percentage of fine aggregates, including powder (< 0.075 mm), %. P_a is the asphalt-aggregate ratio %. ρ_{cs} is the stacking density of coarse aggregate, g/cm^3. ρ_f is the bulk density of fine aggregates, g/cm^3. ρ_a is the density of asphalt binder, g/cm^3.

2.4. Design and performance evaluation of rubberised epoxy asphalt mixtures

For the asphalt mixture gradation design, this study adopts limestone with a maximum particle size of 31.5 mm, which aligns with the majority of existing asphalt trackbed research (Fang et al., 2020). The bulk density and apparent density of both coarse and fine aggregates were measured following the wire basket method (T 0304-2005) and the flask method (T 0328-2005), respectively, as specified in JTG E42-2005 (China, 2005). The measured results can be found in Table 2.

To improve the toughness of the epoxy asphalt, SBS modified asphalt binder with a 4% SBS content was employed. The epoxy system consists of epoxy resin and curing agent, with a mass ratio of 56:44. The mass ratio of the epoxy curing system to the SBS modified asphalt is 1:1. The density of the epoxy asphalt was determined in accordance with the specification JTG E20-2011 (China, 2011), yielding a value of 1.05 g/cm^3. To improve the elastic recovery and damping performance of asphalt mixture, the 4.75-mm CR produced from waste tires with 1.02 g/cm^3 in density was selected to prepare the mixtures.

Theoretical gradation and volume parameters of coarse aggregates: To determine the gradation of coarse aggregates, the volume filling ratio (V_0) of the coarsest aggregate (26.5–31.5 mm) was tested under a single particle size condition. According to JTG E42-2005 (T0309-2005) (China, 2005), a compacted density test was performed using a 10 L testing container, yielding a result of 1.67 g/cm^3. The apparent density of the 26.5 mm aggregate was measured at 2.88 g/cm^3. Using Equation (3), the V0 under the single particle size condition was calculated, leading to the theoretical gradation of coarse aggregates as shown in Table 3. The calculation results indicate that the 4.75 mm aggregate has the highest volume proportion. Previous studies have shown that the retention rate of the 4.75 mm aggregate fraction is the highest, providing better protection for larger-sized aggregates (Li, Shang, Liu, et al., 2019a, 2019b).

Equation (8) relates to the volume parameters VCA and the synthetic bulk density of coarse aggregate. To calculate VCA after the formation of the coarse aggregate skeleton, the synthetic bulk density and compacted density of the coarse aggregate must be measured. Using the theoretical gradation

Table 2. Density of various grades of aggregate(g/cm^3).

Sieve size / mm	26.5	19.0	16.0	13.2	9.5	4.75	≤1.18	Filler
Density/ (g/cm^3)	2.82	2.69	2.70	2.63	2.64	2.55	2.73	2.57

Table 3. Design of epoxy asphalt mixture gradation with different CR contents.

Sieve size/ mm	26.5	19.0	16.0	13.2	9.5	4.75	CR	1.18	0.6	0.3	0.15	0.075	Filler
Percentage retained of coarse aggregates /%	18.3	13.1	12.2	13.2	17.7	25.4	–	–	–	–	–	–	–
Percentage retained of fine aggregates /%	–	–	–	–	–	–	–	26.8	19.2	14.5	10.6	7.8	21.2
Ratio of coarse to fine aggregates/%	73.0	–						27.0					
EA-0CR	13.25	9.50	8.86	9.58	12.79	18.53	0	7.41	5.31	4.00	2.93	2.14	5.86
EA-2CR						13.54	2						
EA-4CR						8.54	4						
EA-6CR						3.54	6						

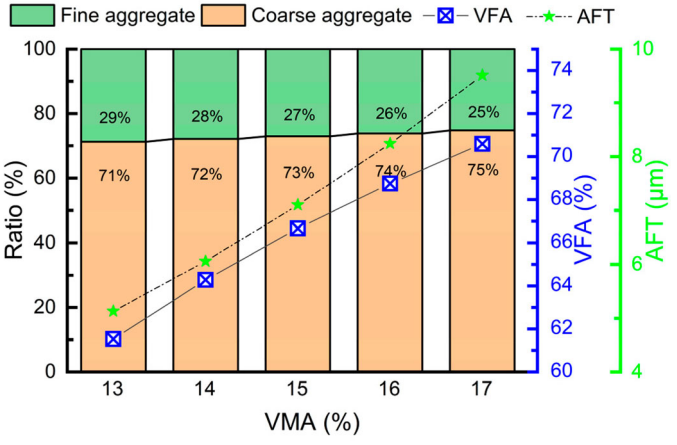

Figure 4. The influence of VMA on the aggregate composition, AFT and VFA.

and the bulk density data from Table 2, the synthetic bulk density of the coarse aggregate is calculated as 2.66 g/cm^3. The compacted density of the coarse aggregate is determined to be 1.64 g/cm^3. Therefore, VCA $=$ (1–1.64/2.66) $*$ 100% $=$ 38.31%.

Theoretical gradation and volume parameters of fine aggregate: The theoretical gradation of the fine aggregate can be obtained using Equation (6), as shown in Table 3. The synthetic density of the mixed fine aggregate is calculated to be 2.69 g/cm^3.

Determination of VV and VMA Parameters: The selection of volume parameters significantly affects the durability of asphalt mixtures, and the specifications JTG F40-2004 provide guidelines for VV and VMA (China, 2004; Zhang et al., 2023). Typically, the recommended VV for asphalt pavement mixtures is 4%. However, this study aims to establish an elastic concrete system, necessitating the addition of deformable CR to increase toughness and reduce the strength of the epoxy asphalt mixture. To accommodate the deformation of CR adequately, the VV is set to 5% in this study. Based on the determined VV and nominal maximum aggregate size, the recommended VMA should not be less than 13%. Related studies suggest increasing VMA by 2%—4% to achieve a higher VMA for a skeleton-type asphalt mixture (Li, Shang, Liu, et al., 2019a, 2019b). Herein, VMA is set at 13–17% to investigate its impact on aggregate proportion and physical parameters. The AFT and VFA values are calculated using the methods described in (Al-Khateeb, 2016), as shown in Figure 4. According to the study conducted by NCHRP 673, an AFT value ranging from 7 to 9 μm demonstrates good construction workability and performance on the road (Board et al., 2011). The recommended VFA range in JTG F40-2004 is 55–70%, making the selectable VMA values 15% and 16%.

When designing according to the V-S method, the oil absorption characteristics of the aggregates are not considered, and only the effective asphalt content is taken into account. The amount of asphalt absorbed by the aggregates can be calculated using Equation (10). This results in total binder-to-aggregate ratios of 3.84 and 4.17 for VMA values of 15% and 16%, respectively.

$$P_{ba} = \frac{\gamma_{se} - \gamma_b}{\gamma_{se} \times \gamma_{sb}} \times \gamma_b \times 100\% \tag{10}$$

where γ_{se} represents the effective relative density of mineral aggregate, which is calculated according to Equations (11)–(13). γ_{sb} represents the synthetic relative bulk specific gravity of the mixture, and γ_b represents the relative density of the asphalt binder.

$$\gamma_{se} = C \times \gamma_{sa} + (1 - C) \times \gamma_{sb} \tag{11}$$

$$C = 0.033w_x^2 - 0.2936w_x + 0.9339 \tag{12}$$

$$w_x = \left(\frac{1}{\gamma_{sb}} - \frac{1}{\gamma_{sa}}\right) \times 100\% \tag{13}$$

where C is asphalt absorption coefficient, dimensionless; w_x is synthetic mineral coefficient rate, %.

Marshall stability tests were performed on asphalt mixtures designed with VMA values of 15% and 16%. The obtained stability and flow values were 32.3 and 30.1 kN, with flow values of 3.5 and 4.2 mm, respectively. It was observed that lower VMA values led to increased strength and reduced deformation. Therefore, for this study, a VMA value of 15% was chosen. Following the principle of equal volume replacement, CR was used to replace coarse aggregates of the same particle size. The density ratio between the replaced aggregates and CR was 2.49. The mass percentage of CR needed to replace the entire batch of 4.75-mm aggregates was determined to be 7.4%. In order to achieve elastic control of epoxy asphalt mixtures, four different mixtures were designed with CR mass percentages of 0%, 2%, 4%, and 6% (equivalent to volume ratios of CR in mineral aggregates of 0%, 5.2%, 10.5%, and 15.7%). These mixtures were labelled as EA-0CR, EA-2CR, EA-4CR, and EA-6CR, respectively. The theoretical gradations of these mixtures can be found in Table 3. Considering the phenomenon of CR adsorbing light asphalt components and swelling in asphalt, the optimal bitumen-to-stone ratio for EA-2CR, EA-4CR, and EA-6CR was determined through marshall test based on EA-0CR. This resulted in ratios of 4.3%, 4.7%, and 5.3%, respectively.

Indoor performance tests, including marshall test, water stability test, high-temperature stability test, and low-temperature bending test, were conducted based on the designed gradation and curing method of epoxy asphalt mixtures with different CR contents. The technical requirements proposed by the specification GB T30598-2014 (General Administration of Quality Supervision, 2014) were referred to for evaluation. The results, shown in Figure 5, indicate that all performance indicators meet the requirements for epoxy asphalt mixtures used in pavement layers, except for the slightly unsatisfactory stability and flow values of EA-6CR. Considering the lower stress values in the track structure, further analysis of the mechanical properties of EA-6CR will be conducted.

3. Feasibility analysis and performance evaluation of rubberised epoxy asphalt trackbed

3.1. Finite element method (FEM) modelling

In this study, a 3D finite element (FE) model was created to evaluate the mechanical performance of rubberised epoxy asphalt trackbed. The model, depicted in Figure 6, had a length of 30 m and encompassed the working area of 50 sleepers. For a detailed description and parameters of the FE model, please refer to Ref. (Shi et al., 2021). The coefficients of the eleventh Prony series for the designed rubberised epoxy asphalt mixtures are determined by dynamic modulus tests and related viscoelastic theories. The detailed testing process and results can be found in Ref. (Wu et al., 2023). Meanwhile, the

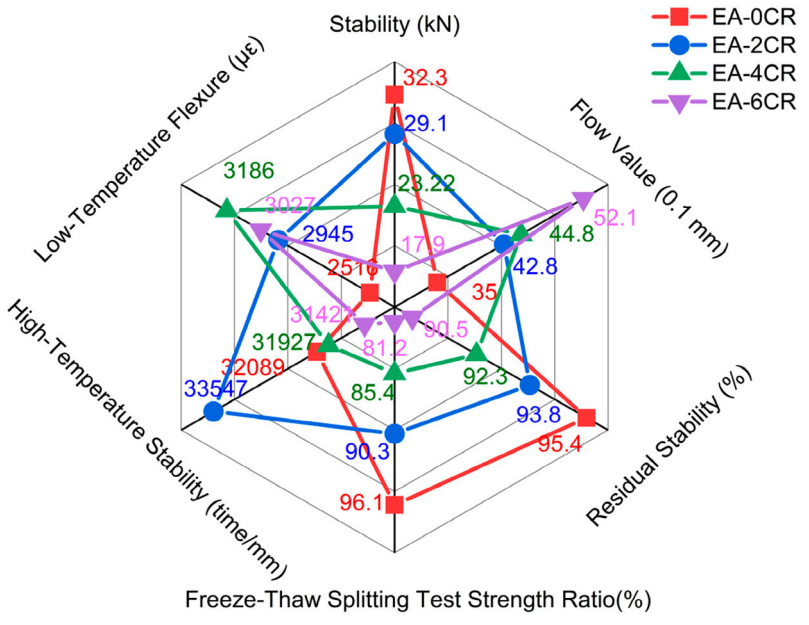

Figure 5. Test results of four rubberised epoxy asphalt mixtures.

damping ratios of the four rubberised epoxy asphalt mixtures were calculated from the mentioned test to be 13.8%, 15.0%, 19.5%, and 21.1%, respectively. These values will subsequently be incorporated into Equation (16) for further evaluation. Additionally, the stiffness calibration and dynamic response calibration of the precast asphalt track FE model have been previously discussed in other studies (Shi et al., 2021; Wu et al., 2023). To simulate the transient dynamic response caused by moving train loading, the dynamic equilibrium governing equation in matrix form can be represented as Equation (14) (Tucho et al., 2022):

$$[M]\{\ddot{U}\} + [C]\{\dot{U}\} + [K]\{U\} = [F] \tag{14}$$

where $[M]$, $[C]$ and $[K]$ represent the mass matrix, damping matrix, and stiffness matrix of the structure, respectively. $\{\ddot{U}\}$, $\{\dot{U}\}$ and $\{U\}$ represent the acceleration vector, velocity vector, and displacement vector of the structure, respectively. $[F]$ represents the load vector of the structure. To characterise the damping characteristics of epoxy asphalt mixtures with different CR contents, this study adopted the commonly used Rayleigh damping in the model. The damping matrix is a linear combination of the mass matrix and the stiffness matrix, as shown in Equation (15):

$$[C] = \alpha[M] + \beta[K] \tag{15}$$

where α and β are proportionality constants related to the natural frequency (ω_1, ω_2) and damping ratio (D) of the track structure, which are calculated according to Equation (16).

$$\begin{Bmatrix} \alpha \\ \beta \end{Bmatrix} = \frac{2D}{\omega_1 + \omega_2} \begin{Bmatrix} \omega_1\omega_2 \\ 1 \end{Bmatrix} \tag{16}$$

The loading of CRH380 high-speed train was simulated and showcased on the FE model (Equation (17)) (Shi et al., 2021; Wu et al., 2023).

$$F(t) = k_1k_2F(t)' = k_1k_2(P_0 + P_1 \sin\omega_1 t + P_2 \sin\omega_2 t + P_3 \sin\omega_3 t) \tag{17}$$

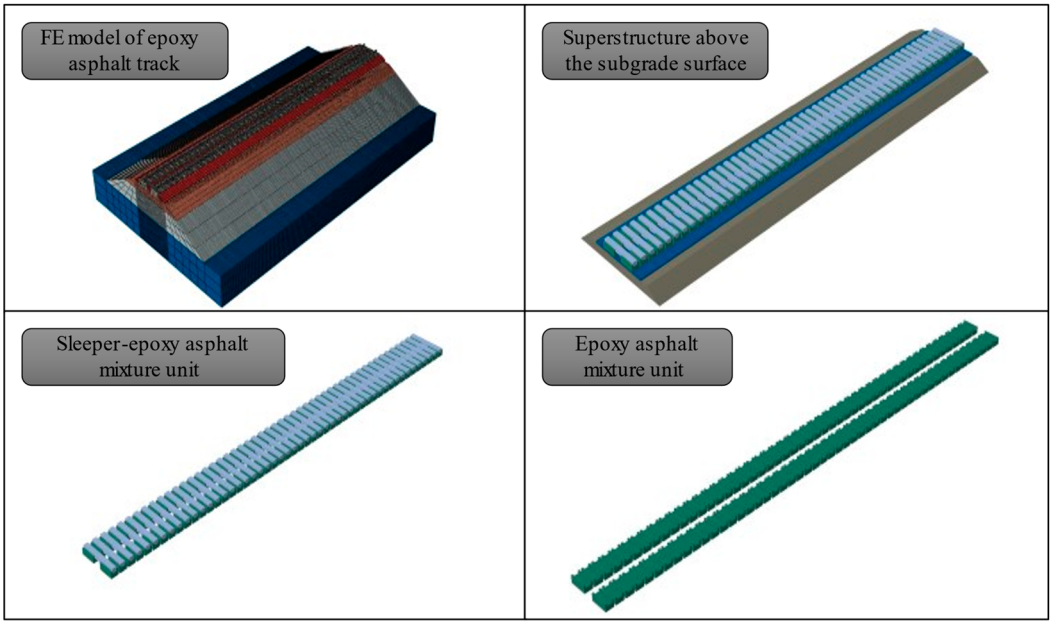

Figure 6. FE model and structure description.

where P_0 is the static wheel load of a wheel, the value of P_0 is 85 kN for the CRH380; $P_i \sin \omega_i t (i = 1, 2, 3)$ presents the vibration loading of train including three parts: train stationary, dynamic additional load and corrugations, $P_i = M_o a_i \omega_i^2$. where M_o is the unsprung weight of the train, 750 kg; a_i and ω_i are the vector height and the circular frequency of the vibration, respectively; ω_i can be determined by $\omega_i = 2\pi v / L_i$, v is the speed of train, 350 km/h; the load model needs to consider a superposition coefficient $k_1 = 1.538$ due to the effect of loading superposition. Meanwhile, the total loading transfers to 5 sleepers, as shown in Figure 2. Therefore, the dispersion coefficient $k_2 = 0.7$ is applied. The modified form of load model is expressed as Equation (18):

$$F(t) = 1.0766 \times (85 + 9.8 \sin 61.1t + 35 \sin 305.4t + 89.6 \sin 1221.7t) \tag{18}$$

3.2. Analysis of mechanical response

This section focuses on analysing the mechanical response of prefabricated epoxy asphalt elastic tracks with different CR contents from tensile strain at the bottom of the asphalt layer, vertical compressive stress, rail foundation modulus, track stiffness, and acceleration in each structural layer.

Figure 7 provides information on the maximum tensile strain in both the transverse (perpendicular to the direction of the train) and longitudinal (direction of the train) directions of the asphalt prefabricated block layer, as well as the maximum vertical compressive stress on the top of the subgrade surface. These results are obtained for four types of epoxy asphalt tracks subjected to a vehicle load travelling at a speed of 350 km/h. The findings indicate that all the designed epoxy asphalt mixtures, with varying CR contents, meet the designated design criteria for trackbed structures. Therefore, these mixtures are suitable for use in high-speed railway track structures.

The addition of CR increases the deformability of the asphalt mixture and reduces the stiffness of the track. As a result, the tensile strain at the bottom of the asphalt trackbed layer increases with higher CR content, but it remains below the fatigue limit strain of the epoxy asphalt mixture, preventing fatigue cracking in the curing blocks. Interestingly, the transverse tensile strain is slightly higher than the longitudinal tensile strain, which differs from the strain state observed in asphalt concrete layers of

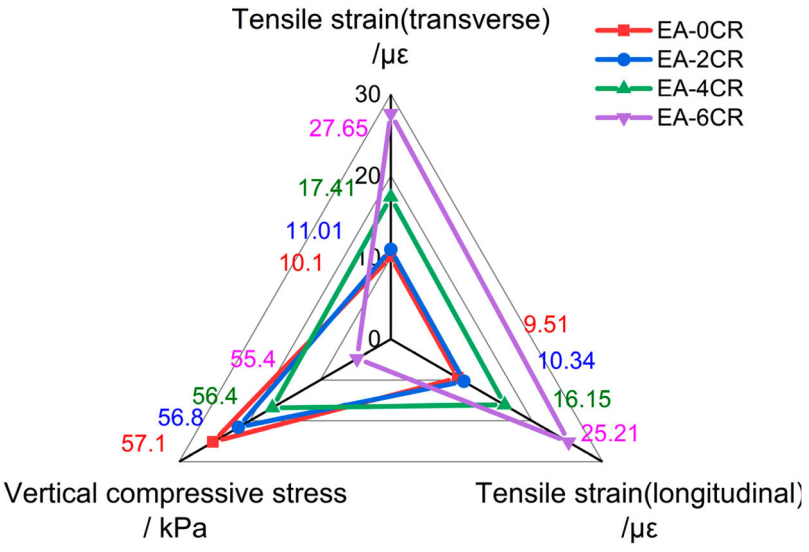

Figure 7. Mechanical response of rubberised epoxy asphalt track.

ballastless tracks (Zhou et al., 2019). Specifically, compared to EA-0CR, EA-2CR shows a smaller increase in bottom tensile strain, while EA-4CR and EA-6CR exhibit increases of 72.4% and 69.7% in transverse tensile strain, and 173.8% and 165.0% in longitudinal tensile strain, respectively. Zania's team conducted a full-scale physical model test on asphalt ballastless track, where sleepers were directly placed on the continuous asphalt pavement structure (Bose et al., 2020, 2021). They applied a vehicle load of 120 kN at speeds of 120 and 200 km/h and measured the tensile strains at the bottom of the asphalt layer. The results showed maximum transverse tensile strains of 20 and 39 $\mu\varepsilon$, as well as a maximum longitudinal tensile strain of 15 and 20 $\mu\varepsilon$. Notably, the transverse tensile strain under the sleepers was higher than the longitudinal tensile strain, which aligns with the findings of this study, validating the finite element model used. Lee's team also conducted full-scale indoor studies using an asphalt concrete layer as a base plate for ballastless track systems (Lee et al., 2016, 2019, 2021, 2023). They applied sinusoidal loads with a vehicle speed of 140 km/h and a dynamic axle load of 175 kN and determined the optimal asphalt layer thickness to be 35 cm, with a maximum tensile strain at the bottom of the layer of 40 $\mu\varepsilon$. Although both teams used ordinary asphalt and lower vehicle speeds compared to this study, the strain values were higher than the numerical simulation results in this research, demonstrating the favourable mechanical behaviour of epoxy asphalt materials in track structures.

Figure 8 illustrates the characteristics of the transverse and longitudinal tensile strains at the bottom of the epoxy asphalt curing blocks at the mid-span of the model using EA-0CR as an example. The maximum tensile strains are observed at the edges of the curing blocks, with the transverse tensile strain decreasing gradually from the centre to the edges and reaching its peak at the edges. On the other hand, the longitudinal tensile strain does not exhibit significant values at the centre of the curing block's bottom but gradually increases towards the sides and reaches its maximum value at the edges. The contour of the tensile strains indicates that the dynamic response of a single axle load is mainly borne by the adjacent five sleepers, suggesting consistency between the dynamic response of the finite element model and the actual stress distribution in the track structure (Bian et al., 2020, 2023).

The vertical compressive stress and deformation on the top of the subgrade ranges from 57.0 to 55.4 kPa, gradually decreasing with increasing CR content, although the attenuation is not significant. In a previous study, Bose et al. conducted FE numerical simulations to analyse the vertical compressive stress in track structures (Bose et al., 2021). They found that the vertical compressive stresses at the top and bottom of the subgrade surface were 27 and 25 kPa, respectively. These values were lower than

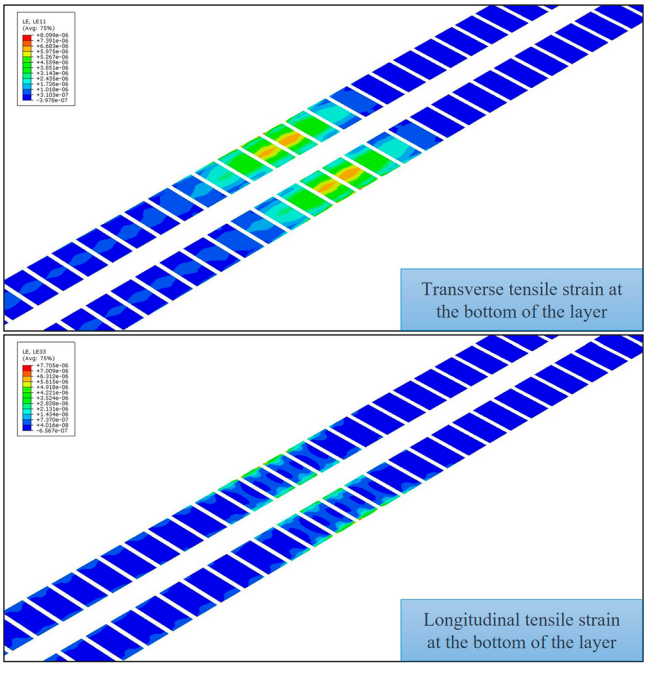

Figure 8. Contour of tensile strain under the asphalt layer.

the stress response observed in our research. However, it should be noted that their load level and vehicle speed were significantly lower than the 350 km/h vehicle speed and 170 kN axle load used in our study. Additionally, despite the subgrade's thickness being only 27.5 cm, the absolute decrease in vertical compressive stress was merely 2 kPa, indicating limited stress dissipation capability. Lee et al. conducted field measurements and obtained a vertical compressive stress of 64.68 kPa on the top of the subgrade surface (Lee et al., 2021). Their research involved an asphalt layer located beneath the concrete track slab, resulting in a more favourable stress condition compared to the epoxy asphalt curing blocks placed under the sleepers. However, their results were slightly higher than those of our study. Similarly, Liu used epoxy asphalt mixture in the sub-ballast of ballastless tracks, replacing the original concrete base plate (Liu et al., 2019). Through finite element numerical simulations, they analysed the mechanical response of the asphalt layers in the ballastless track at a vehicle speed of 350 km/h, observing a vertical compressive stress on the top of the subgrade surface of 15.41 kPa. By comparing the studies of Lee and Liu, it can be concluded that epoxy asphalt mixtures hold promising prospects for application and offer advantages in dynamic response within track structures.

Figure 9 shows the contour of vertical compressive stress on the top of the subgrade surface under train loading. It displays a 'double-block' pattern, with the maximum vertical compressive stress occurring near the edges of the two curing blocks. This stress gradually spreads outward from that region. The concentrated distribution of tensile strains at the bottom of the epoxy asphalt curing blocks and the vertical compressive stress on the top of the subgrade surface near the curing block's edges is due to this area being directly under the rail and serving as the primary region for transferring train loads. The observed pattern of dynamic response holds true for all epoxy asphalt elastic tracks, and therefore, the contour plots and patterns for other trackbeds are not discussed here.

In the continuous support model, the rail is considered as a long beam on a continuous elastic foundation, and the displacement of the load P at the rail is Equation (19):

$$y = \frac{Pk}{2u} \tag{19}$$

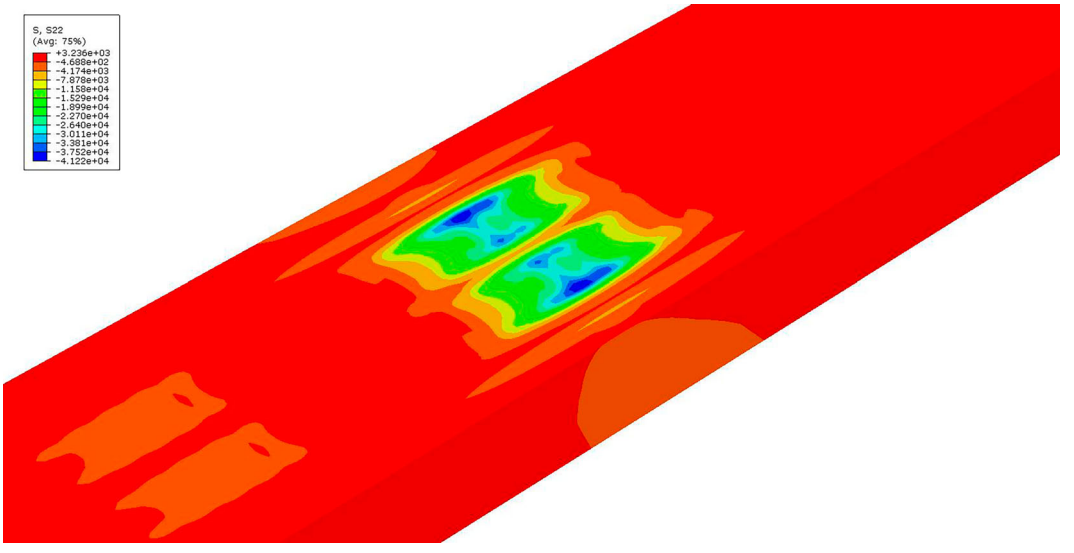

Figure 9. Contour of vertical stress on the top of subgrade surface.

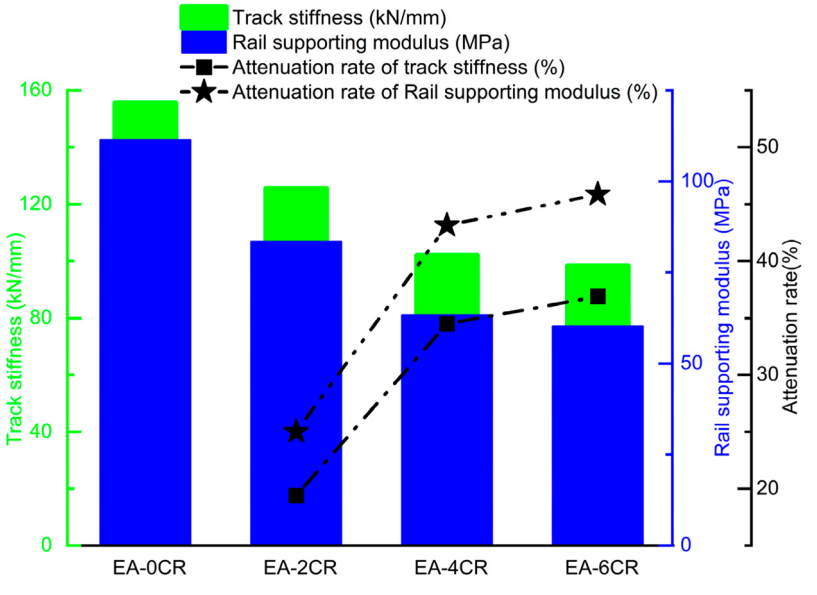

Figure 10. The rail stiffness and rail foundation modulus of epoxy asphalt ballast beds with different CR contents.

where u is rail foundation modulus; k is the stiffness ratio coefficient between the rail foundation and the rail, which is presented as Equation (20):

$$k = \sqrt[4]{\frac{u}{4EI}} \tag{20}$$

The rail stiffness (K) is determined by the load necessary to generate a unit deflection on the rail under a concentrated load, as defined in Equation (21). By integrating Equations (19) to (21), we can establish the correlation between the rail foundation modulus and the rail stiffness, as demonstrated

in Equation (22) (Kankhva et al., 2024; Tong et al., 2022).

$$K = \frac{P}{y} \tag{21}$$

$$u = \sqrt[3]{\frac{K^4}{64EI}} \tag{22}$$

where EI is rail bending stiffness.

This study utilised finite element numerical simulation to calculate the rail stiffness of epoxy asphalt tracks with varying CR contents. The rail foundation modulus was determined using Equation (22), as shown in Figure 10. The rail stiffness ranged from 98.2 to 155.6 kN/mm, while the rail foundation modulus ranged from 60.3 to 111.4 MPa. Adding every 2% CR resulted in attenuation rates of 19.4% and 25.0% (EA-2CR/EA-0CR), 18.7% and 24.2% (EA-4CR/EA-2CR), and 3.6% and 4.8% (EA-6CR/EA-4CR) for the two mechanical indicators, respectively. Notably, EA-4CR exhibited the most optimal performance in terms of increased elasticity and reduced stiffness. It is important to note that a rail foundation modulus greater than 28 MPa (Selig & Li, 1994) is recommended to ensure rail structure stability, a requirement met by all the designed epoxy asphalt tracks. In a separate study, Lee et al. (2021) replaced the base plate of ballastless tracks with an asphalt layer, resulting in a rail stiffness range of 34.1–46.7 kN/mm and a rail foundation modulus of 14.8–21.3 MPa, achieved by adjusting the asphalt layer thickness and load-induced stress level. Bose et al. (2021) placed an asphalt layer beneath the sleepers and recorded a dynamic stiffness range of 32.0–35.0 kN/mm. Both studies used normal asphalt mixtures, and their measured vertical stability indicators were relatively small, potentially impacting the long-term stability of the rail structure. Therefore, epoxy asphalt mixtures are better suited for application in ballastless track base plates and asphalt overlayment beneath the sleepers. Previous research has recommended a vertical overall stiffness range of 61.06–102.69 kN/mm for subway track structures (Li et al. 2018). In this study, the rail stiffness values for EA-4CR and EA-6CR were measured at 101.9 and 98.2 kN/mm, respectively, indicating that these two epoxy asphalt trackbeds are viable options for subway track structures.

In conclusion, the epoxy asphalt mixtures with varying CR contents, as designed in this study, are well-suited for railway track structures and demonstrate superior mechanical properties compared to ordinary asphalt mixtures. To quantify the influence of rubber content on track structure vibration reduction, the next section will analyse the trackbed's vibration behaviour using both time-domain and frequency-domain perspectives of acceleration.

4. Analysis of vibration reduction effect of CR content

4.1. Evaluation of track vibration behaviour

The evaluation and measurement of vibration behaviour in track structures often focus on the temporal and spectral characteristics of acceleration (Ahn et al., 2019; Akiyama et al., 2020; Bashir & Akhtar, 2021). Time-domain analysis provides a way to examine vibration behaviour by studying the temporal changes of physical quantities. On the other hand, frequency-domain analysis involves performing Fourier transforms on the results obtained from time-domain analysis to identify the frequency components of the vibration physical quantities.

(1) Time-Domain Analysis Indicators: Vibration acceleration in the time domain reflects the intensity of vibration loads on track structures caused by train loads. The time history curve of acceleration provides insights into the vibration characteristics experienced by track structures over a specific time period. Key indicators, such as peak acceleration, are used to comprehensively analyse the attenuation patterns of vertical vibrations across different structural layers in the track.

(2) Frequency-Domain Analysis Indicators: While time-domain analysis has limitations in evaluating vibration characteristics, frequency-domain analysis, particularly acceleration spectrum analysis, is widely used. It reveals the relative strength and contribution of different frequency components in the signal. The relationship between vibration acceleration level and the 1/3-octave band of acceleration is employed to analyse vibration intensity in different frequency ranges of track structures. To establish this relationship, the following process is necessary:

(a) a. Vibration Acceleration Level (VAL): To overcome the inconvenience of measuring and characterising vibration using absolute acceleration values that can vary significantly, the concept of VAL is introduced as a representation of vibration characteristics. It is defined as Equation (23) (Shan et al., 2021):

$$VAL = 20 \lg \frac{a}{a_0} \tag{23}$$

Once the VAL is obtained, the Insertion Loss (IL) between different track structures can be calculated using Equation (24). IL serves as a parameter for analysing the impact of different track structure forms or vibration damping materials on the vibration characteristics of track structures.

$$\begin{aligned} L_{IL} &= 20 \lg \frac{I_1}{I_2} = 20 \lg \frac{a_1}{a_2} \\ &= 20 \lg \frac{a_1}{a_0} \cdot \frac{a_0}{a_2} = VAL_1 - VAL_2 \end{aligned} \tag{24}$$

where a is the effective value of the vibration acceleration, m/s^2; a_0 is the reference acceleration, which is generally taken as 10^{-6}m/s^2.

b. One-third Octave Band: The one-third octave band offers a more detailed frequency resolution and broader spectrum coverage without overwhelming data volume or complexity in analysis.

4.2. Time-domain investigation of vibration mitigation

By analysing the vibration acceleration data collected from various components in the epoxy asphalt track, the influence of CR content on the temporal domain signals of acceleration at the top positions of the rail (Position 1, P1), sleeper (Position 2, P2), and epoxy asphalt curing blocks (Position 3, P3) and at the bottom of epoxy asphalt curing blocks (Position 4, P4) was examined. Figure 11 presents a comparative diagram of the typical vibration acceleration time history curves on the top of the rail for four epoxy asphalt track structures. Initially, the acceleration is minimal at the data collection point in the middle of the model. However, as the vehicle load approaches the collection point, the acceleration gradually increases, alternating in the positive and negative directions. Overall, the acceleration at different components of the track structure decreases with an increase in CR content. The range of acceleration values is summarised in Table 4, and the maximum acceleration values at the rail locations meet the safety and passenger comfort requirements specified in TB10761-2013 (China, 2013). The time history curves of acceleration at the same layer position of the track structure exhibit a high degree of similarity. The maximum downward and upward acceleration values of the rail occur at 0.137s and 0.139s, respectively, with the absolute value of the downward acceleration being greater than the upward acceleration. This finding is consistent with a previous study (Liu et al., 2019) that compared two track structure forms: CRTS-I ballastless track and a variation that replaced the base plate with an epoxy asphalt layer. The numerical simulation showed maximum rail vibration acceleration values of -184.32 g and -175.46 g, respectively, indicating that the replacement of the base plate with an epoxy asphalt layer effectively reduces rail vibration. Comparing these results with the present study, it is evident that the use of an epoxy asphalt layer directly under the sleeper, regardless of the addition of CR, effectively reduces rail vibration. The maximum rail vibration acceleration values for

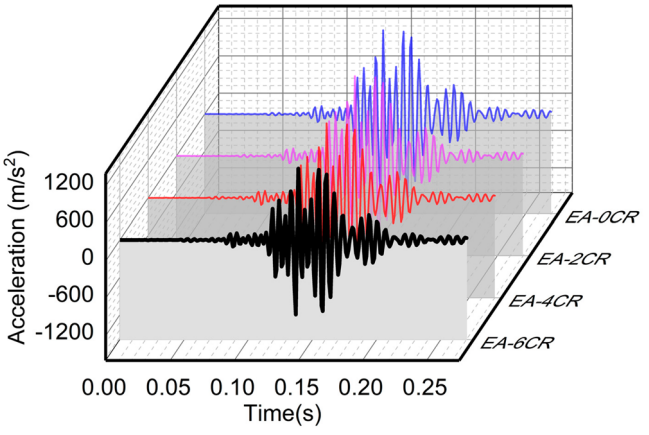

Figure 11. Acceleration time history curve at the top of the rail.

Table 4. Acceleration range of various track components.

Acceleration/ (m/s^2)	P1	P2	P3	P4
EA-0CR	[−1406.15, 1347.14]	[−31.50, 38.09]	[−17.43, 22.67]	[−14.53, 17.13]
EA-2CR	[−1341.00, 1284.06]	[−30.61, 36.88]	[−16.99, 21.95]	[−12.60, 14.83]
EA-4CR	[−1253.23, 1199.51]	[−29.04, 35.04]	[−16.39, 20.85]	[−11.38, 14.01]
EA-6CR	[−1196.14, 1144.27]	[−27.62, 33.45]	[−16.10, 19.90]	[−11.20, 13.16]

the four types of precast epoxy asphalt track structures are -140.6, -134.1, -125.3, and -119.6 g, respectively, significantly lower than the standards' requirements of 500 g (for ballastless track) and 300 g (for ballasted track) (China, 2013). When the train load is transmitted to the sleeper and epoxy asphalt layer, the maximum upward acceleration occurs before the maximum downward acceleration, with the upward acceleration being greater. This contrasts with the results observed at the top of the rail. In epoxy asphalt layers with different CR contents, the peak acceleration at the top of the sleeper is significantly lower than the threshold specified in the standards (50 g), and the peak acceleration at the top of the epoxy asphalt curing blocks is much lower than the standards' requirements (30 g).

The acceleration experiences a sharp decrease from the top of the rail to the top of the sleeper, with an attenuation rate of approximately 97.2%. The attenuation rate from the top of the sleeper to the top of the curing block is around 40.5% due to the consistent use of rail, fasteners, and sleepers in all four types of epoxy asphalt track. As the acceleration is transmitted from the top of the epoxy asphalt curing blocks to the bottom of that, the attenuation rates are 24.44% (EA-0CR), 32.42% (EA-2CR), 32.63% (EA-4CR), and 33.88% (EA-6CR) respectively. The addition of CR significantly enhances the vibration dissipation and transmission in the asphalt layer. The attenuation rate of acceleration in the curing block increases with the increase in CR content. Figure 12 illustrates the peak acceleration attenuation rates at the same component layer for different mass percentages of CR. Each 2% increase in CR content results in a convex peak of attenuation rates at the top of the rail, top of the sleeper, and top of the curing block. The maximum attenuation capacity occurs when the CR content increases from 2% to 4%. However, the bottom of the curing block shows the opposite trend, with the maximum attenuation of peak acceleration immediately after the addition of CR, reaching an attenuation value of 13.4%. In conclusion, the peak acceleration exhibits the highest attenuation rate at a CR content of 4%, indicating the optimal increase in vibration reduction performance.

4.3. Frequency domain investigation of vibration mitigation

The VAL in the 1/3-octave frequency range exhibits a three-stage distribution (as shown in Figure 13): stability in the low-frequency range (1–2.5 Hz), gradual increase in the mid-to-high-frequency range

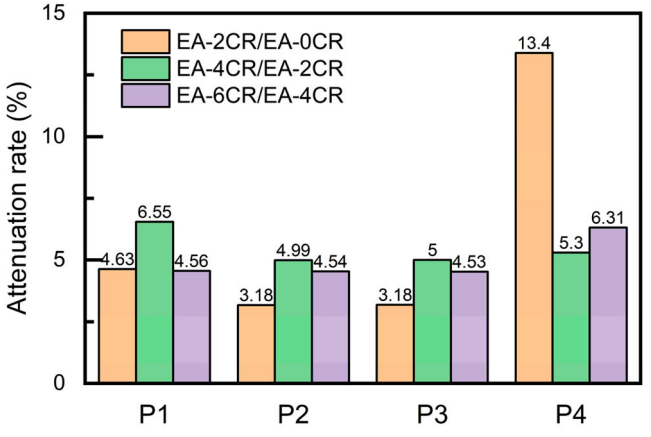

Figure 12. Attenuation rate of peak acceleration.

(2.5–200 Hz), and sharp decrease in the high-frequency range (200–400 Hz). This pattern aligns with the analysis results of measured data for polyurethane curing trackbed (Xing, 2021). Overall, the VAL of various components in epoxy asphalt track structures remains relatively consistent as the frequency increases in the low-frequency range. The differences in VAL between EA-0CR and EA-6CR from the rail to the bottom of the curing block are 1.41, 1.52, 1.30, and 3.97 dB, respectively. The bottom of the curing block exhibits the most significant vibration reduction effect within the trackbed structure, indicating that the addition of CR enhances the overall damping performance of the epoxy asphalt track. In the mid-to-high-frequency range, the VAL on the rail increases at a faster rate than the other three components. The VAL at the top and bottom of the curing block is relatively consistent between EA-0CR and EA-2CR, suggesting that a 2% CR content is insufficient to alter the damping performance of pure epoxy asphalt mixture. However, the VAL differences between EA-4CR, EA-6CR, and EA-0CR at the top and bottom of the curing block range from 2.60 to 5.64 dB and from 2.65 to 5.26 dB, respectively, indicating that a CR content of 4% and 6% significantly enhances the vibration reduction performance of the epoxy asphalt track. The trend of VAL at the sleeper follows the overall trend observed at the top and bottom of the curing block.

To assess the impact of CR content on the damping behaviour of the epoxy asphalt track, the VAL differences between EA-2CR, EA-4CR, EA-6CR, and EA-0CR were calculated at the same component and the same 1/3-octave frequency centre. These differences, known as Insertion Loss (IL), provide insight into vibration reduction, as shown in Figure 14. In this study, EA-0CR serves as the reference representing a structure without vibration reduction treatment. Negative IL values indicate effective vibration reduction. At the top of the rail, the IL values consistently remain negative across the frequency range. The average IL values for EA-2CR, EA-4CR, and EA-6CR are -0.43 dB, -1.02 dB, and -1.41 dB, respectively, demonstrating that adding CR enhances vibration reduction at the top of the rail. For the sleeper, slight increases in vibration intensity are observed at 315 Hz for EA-4CR and EA-6CR, while EA-2CR exhibits the maximum IL at this frequency, indicating optimal vibration reduction. At other frequencies, IL values are negative and relatively stable in the 1–20 Hz range, followed by a decreasing trend. EA-2CR shows the highest IL across the entire frequency range. At the top of the curing block, IL values show minimal variation in the 1–100 Hz range, with notable changes occurring only at higher frequencies. Positive IL values are observed at 250 Hz for all cases, and EA-4CR also exhibits a positive IL at 315 Hz, indicating increased vibration intensity at these frequencies. Notably, all cases demonstrate significant IL at 400 Hz, indicating optimal vibration reduction. Among the three cases, EA-2CR exhibits the best vibration reduction behaviour within this frequency range. At the bottom of the curing block, all three cases demonstrate optimal vibration reduction at 400 Hz. The IL trends of EA-4CR and EA-6CR closely align, displaying increasing-decreasing-increasing patterns with peaks exceeding

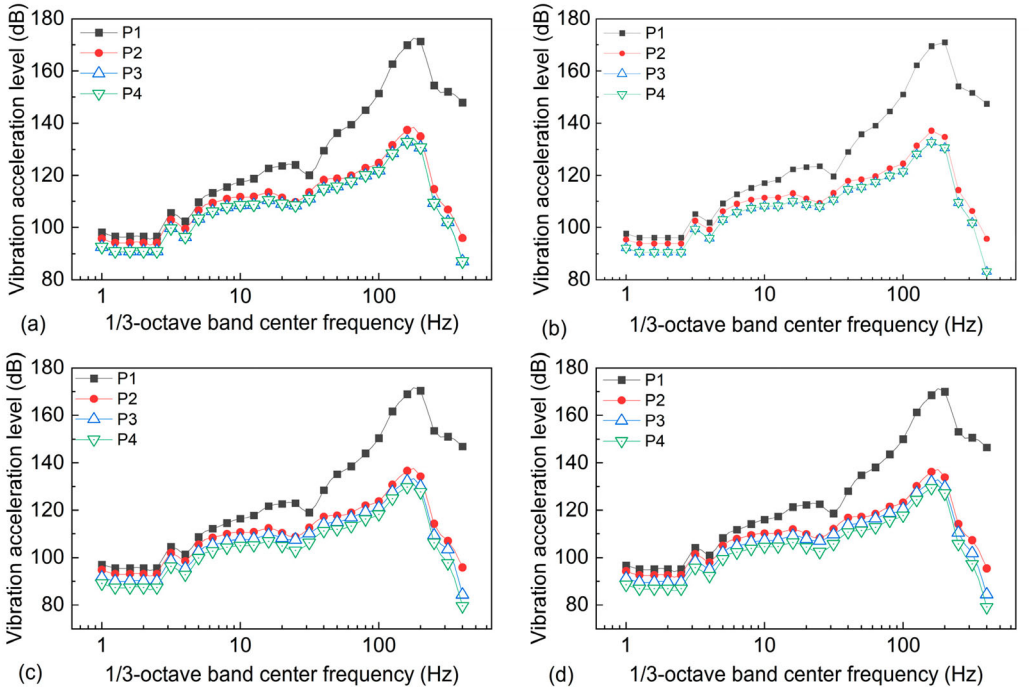

Figure 13. Relationship between VAL and 1/3-octave frequency distribution: (a) EA-0CR, (b) EA-2CR, (c) EA-4CR and (d) EA-6CR.

3 dB, signifying effective vibration reduction. While EA-2CR exhibits enhanced vibration at 250 Hz, its IL values in other frequency domains are negative and relatively similar. Overall, higher CR content leads to increased IL values, indicating improved vibration reduction performance.

The impact of adding every 2% CR on the vibration reduction behaviour of each component of the epoxy asphalt track can be analysed by calculating the IL between the two adjacent trackbeds. For example, EA-2CR represents the IL between the EA-2CR and EA-0CR. The IL values at the rail remain consistent across the entire frequency range, with average values of -0.42 dB (EA-2CR), -0.59 dB (EA-4CR), and -0.40 dB (EA-6CR). Among the cases with the same increase in CR content, EA-4CR demonstrates the best vibration reduction performance. At the top of the sleeper, the IL values remain relatively constant in the 1–125 Hz range, with average values of -0.34 dB, -0.65 dB, and -0.50 dB. In the 160–400 Hz range, EA-2CR exhibits the highest negative IL at 315 Hz, but its absolute value is smaller than that of EA-4CR. However, the other two cases show positive IL at this frequency, indicating increased vibration intensity. Similarly, at the top of the curing block, the IL values remain relatively constant in the 1–160 Hz range, with average values of -0.36 dB, -0.47 dB, and -0.43 dB. All three cases demonstrate the lowest IL at 400 Hz (EA-2CR), 200 and 315 Hz (EA-4CR), and 315 and 400 Hz (EA-6CR), indicating optimal vibration reduction performance. However, positive IL values occur at 250 Hz (EA-2CR), 315 and 400 Hz (EA-4CR), and 315 and 400 Hz (EA-6CR), indicating enhanced vibration effects at these frequencies.

Overall, EA-4CR exhibits the most significant improvement in vibration reduction performance at the bottom of the curing block across the entire frequency range, with IL exceeding 2.83 dB in absolute value. Considering the results of acceleration indicators in both the time and frequency domains for various components of the track structure, the vibration reduction performance of the epoxy asphalt track improves with an increase in CR content. Among the cases with the same increment in CR content, the components of EA-4CR demonstrate better vibration reduction performance.

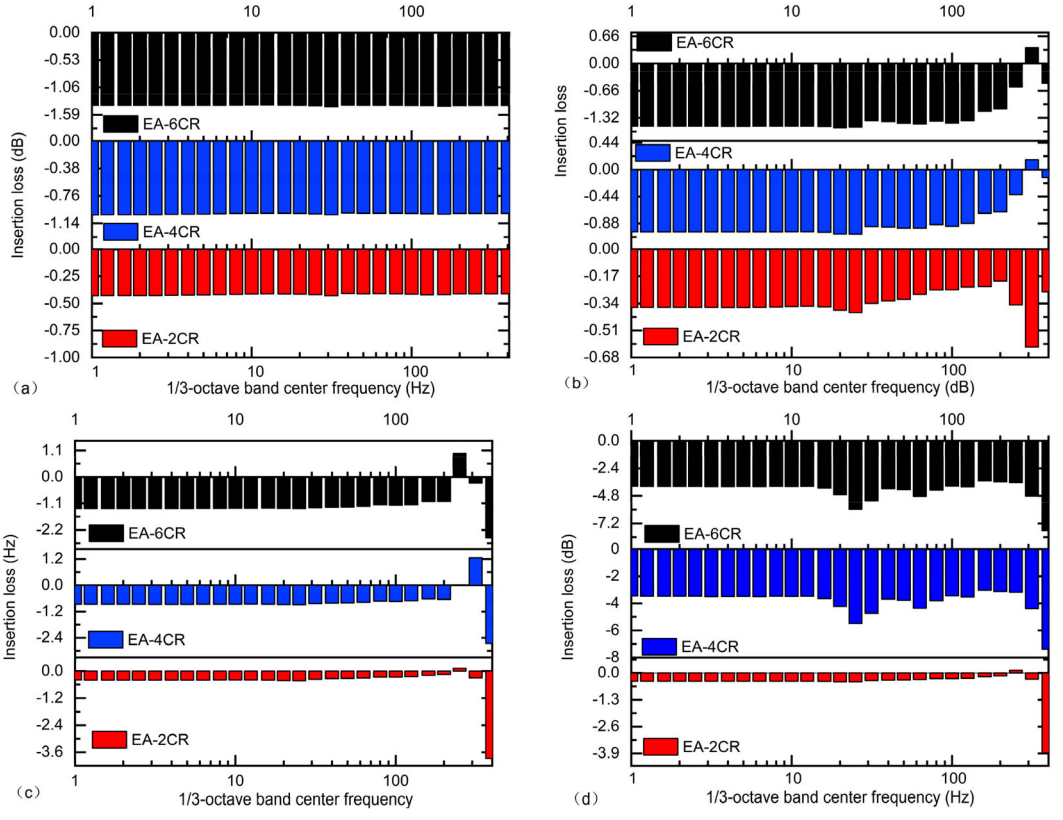

Figure 14. IL: (a) on the top of rail, (b) on the top of sleeper, (c) on the top of asphalt layer, and (d) under the bottom of asphalt layer.

5. Summary and conclusions

This study focuses on designing and investigating the rubberised epoxy asphalt elastic track, specifically examining the impact of CR content on vibration attenuation in the precast epoxy asphalt trackbed. The V-S method was enhanced to consider CR swelling, and four types of rubberised epoxy asphalt mixtures were designed using the modified volumetric mix-design method. FE numerical modelling was employed to analyse the feasibility and damping performance of the designed epoxy asphalt track in both the time and frequency domains. The main findings and conclusions are as follows:

i. The designed rubberised epoxy asphalt track meets the design criteria for railway bituminous trackbeds, ensuring no fatigue cracking, maintaining track regularity, and improving vibration attenuation in railway tracks.
ii. The addition of CR effectively reduces rail stiffness and rail foundation modulus, achieving the desired toughening and elasticating of the epoxy asphalt trackbed. Among the four types of rubberised epoxy asphalt tracks, EA-4CR exhibits optimal performance in terms of increased elasticity and reduced stiffness. The rail foundation modulus of all four tracks exceeds 28 MPa, indicating reliable vertical stability. Furthermore, the EA-4CR and EA-6CR track structures show potential for use in subway tracks.
iii. The maximum acceleration values at the top of the rail, sleeper, and trackbed meet specification requirements. As the dosage of CR increases, the peak vibration accelerations at various components of the track structure decrease, with the EA-4CR track demonstrating the best vibration attenuation performance.

iv. The acceleration spectrum exhibits distinct dual-peak characteristics, with the second main frequency higher than the first main frequency for the rail, and the reverse trend for other components like the sleeper and epoxy asphalt blocks. The VAL shows a three-stage distribution in the 1/3-octave frequency range, with significant vibration attenuation at 400 Hz. Notably, the EA-4CR track exhibits the most significant enhancement in vibration reduction performance at the bottom of the curing blocks, with an IL exceeding 2.83 dB compared to EA-2CR and 3.02 dB compared to EA-0CR.

Considering the results of acceleration indicators in both the time and frequency domains for various components of the track structure, the damping performance of the epoxy asphalt track improves with an increase in CR content. Among the various incremental amounts of CR content, the components of the EA-4CR track structure show superior damping performance. These findings suggest that the rubberised epoxy asphalt track can be applied in railway structures, and the four types of stiffness-gradient rubberised epoxy asphalt tracks have potential use in specific projects, such as transition zones in high-speed railways.

Disclosure statement

The authors declare that they have no known competing financial interests or personal relationships that could have appeared to influence the work reported in this paper.

Funding

This work was supported by Scientific Research Foundation of Graduate School of Southeast University [grant number YBPY2158]; National Natural Science Foundation of China [grant number 52078130, 52378444]; echnology Research and Development Program of China State Railway Group Co., Ltd [grant number P2019G030]; China Scholarship Council program [grant number 202106090047].

CRediT authorship contribution statement

Chenguang Shi: conceptualisation, methodology, formal analysis, investigation, writing-original draft, visualisation. You Wu: methodology, formal analysis. Raul Fuentes: writing-review & editing, supervision. Yulou Fan: methodology, data curation. Yixin Zhou: data curation. Chaoliang Fu: formal analysis. Jun Yang: writing-review & editing, funding acquisition, resources, supervision.

References

Ahn, S., Kwon, S., Hwang, Y.-T., Koh, H.-I., Kim, H.-S., & Park, J. (2019). Complex structured polymer concrete sleeper for rolling noise reduction of high-speed train system. *Composite Structures*, *223*.

Akiyama, Y., Tomioka, T., Takigami, T., Aida, K.-I., & Kamada, T. (2020). A three-dimensional analytical model and parameter determination method of the elastic vibration of a railway vehicle carbody. *Vehicle System Dynamics*, *58*(4), 545–568. https://doi.org/10.1080/00423114.2019.1590606. Available from: < Go to ISI > ://WOS:000518211900003.

Al-Khateeb, G. G. (2016). Conceptualizing the asphalt film thickness to investigate the superpave vma criteria. *International Journal of Pavement Engineering*, *19*(11), 957–965. https://doi.org/10.1080/10298436.2016.1224414

Alves, T. D. F., Moraes Pereira, P. A., Motta, R., Vasconcelos, K., Teixeira, J. L., & Bernucci, L. (2022). Three-dimensional numerical modelling of railway track with varying air voids content bituminous subballast. *Road Materials and Pavement Design*, *23*(2), 414–432. https://doi.org/10.1080/14680629.2020.1828150. Available from: < Go to ISI > ://WOS:000575990200001.

Bashir, S., & Akhtar, N. (2021). Development of low-frequency mass spring system for underground high-speed railways. *Journal of Vibration Engineering & Technologies*, *10*(2), 559–579. https://doi.org/10.1007/s42417-021-00392-w

Bian, X., Gao, Z., Luo, X., Cai, D., & Chen, Y. (2023). Mesoscale mechanism of asphalt track bed in reducing cyclic settlement of ballast layer under high-speed train traffic loads. *Journal of Transportation Engineering Part B-Pavements*, *149*(1), 1–20. https://doi.org/10.1061/JPEODX.0000402

Bian, X., Li, W., Qian, Y., & Tutumluer, E. (2020). Analysing the effect of principal stress rotation on railway track settlement by discrete element method. *Géotechnique*, *70*(9), 803–821. https://doi.org/10.1680/jgeot.18.P.368

Board, T.R., National Academies of Sciences, E. & Medicine. (2011). *A manual for design of hot-mix asphalt with commentary*. The National Academies Press.

Borges Miranda, H. M., Batista, F. A., Neves, J., & Antunes, M. D. L. (2021). Influence of the aggregate skeleton matrix and volumetric composition on the resistance of stone mastic asphalt to permanent deformation. *Road Materials and Pavement Design*, *22*(11), 2538–2551. https://doi.org/10.1080/14680629.2020.1773303. Available from: < Go to ISI > ://WOS:000542876500001.

Bose, T., Levenberg, E., & Zania, V. (2021). Numerical modeling of a ballastless track mockup based on asphalt. *Construction and Building Materials*, *274*, 1–18. https://doi.org/10.1016/j.conbuildmat.2020.121852

Bose, T., Zania, V., & Levenberg, E. (2020). Experimental investigation of a ballastless asphalt track mockup under vertical loads. *Construction and Building Materials*, *261*, 1–15. https://doi.org/10.1016/j.conbuildmat.2020.119711

Bressi, S., D'angelo, G., Santos, J., & Giunta, M. (2018). Environmental performance analysis of bitumen stabilized ballast for railway track-bed using life-cycle assessment. *Construction and Building Materials*, *188*, 1050–1064. https://doi.org/10.1016/j.conbuildmat.2018.08.175. Available from: < Go to ISI > ://WOS:000447579600093.

Castro, G., Pires, J., Motta, R., Bernucci, L., Fortunato, E., & Futai, M. (2022). Evaluating environmental effects on the structural behavior of the railroad track subgrade considering different sub-ballast design solutions. *Transportation Geotechnics*, *34*, 1–18.

China, M.R. (2013). *Technical regulations for dynamic acceptance for high-speed railways construction*. China Railway Publishing House.

China, M.R. (2014). *Code for design of high speed railway*. China Railway Publishing House.

China, M.T. (2004). *Techanical specification for construction of highway asphalt pavements*. China Communications Press.

China, M.T. (2005). *Test methods of aggregate for highway engineering*. China Communications Press.

China, M.T. (2011). *Standard test methods of bitumen and bituminous mixtures for highway engineering*. China Communications Press.

Di Mino, G., & Di Liberto, C. M. (2012). Experimental survey on dry asphalt rubber concrete for sub-ballast layers. *Journal of Civil Engineering and Architecture*, *6*(12), 1615–1626.

Esmaeili, M., Heydari-Noghabi, H., & Sayadi, A. (2018). Field investigation on the lateral resistance of railway tracks including hot mix asphalt layer. *Road Materials and Pavement Design*, *19*(1), 154–166. https://doi.org/10.1080/14680629.2016.1250666

Fang, M., Hu, T., & Rose, J. G. (2020). Geometric composition, structural behavior and material design for asphalt trackbed: A review. *Construction and Building Materials*, *262*, 1–13.

Fang, M., Park, D., Singuranayo, J. L., Chen, H., & Li, Y. (2019). Aggregate gradation theory, design and its impact on asphalt pavement performance: A review. *International Journal of Pavement Engineering*, *20*(12), 1408–1424. https://doi.org/10.1080/10298436.2018.1430365. Available from: < Go to ISI > ://WOS:000487857600005.

Fang, M., Wu, S., Park, D., Chen, H., & Xie, J. (2017). Simple test study on anti-freeze additives selection for railway asphalt mixture (ram) in cold region. *Construction and Building Materials*, *154*, 284–293. https://doi.org/10.1016/j.conbuildmat.2017.07.212. Available from: < Go to ISI > ://WOS:000413056200028.

General Administration of Quality Supervision, I.a.Q.O.T.P.S.R.O.C. (2014). General specifications of epoxy asphalt materials for paving roads and bridges.

Jadidi, K., Esmaeili, M., Kalantari, M., Khalili, M., & Karakouzian, M. (2021). A review of different aspects of applying asphalt and bituminous mixes under a railway track. *Materials*, *14*(1), 1–21. https://doi.org/10.3390/ma14010169

Jin, M. (2017). *The research on epoxy asphalt used in long-life asphalt pavements*. Beijing University of Civil Engineering and Architecture.

Kankhva, V. S., Begmatov, N., & Ergashev, U. (2024). Determination of the modulus of elasticity of railway track with bf70 sleepers. *E3S Web of Conferences*, *515*(02003), 1–7.

Khairallah, D., Chupin, O., Blanc, J., Hornych, P., & Piau, J.-M. (2022). Simulation of the dynamic response of high-speed line structures composed of granular or bituminous sub-ballast layers and comparison with in situ measurements from embedded instrumentation. *Transportation Geotechnics*, *35*, 1–14.

Lee, S.-H., Choi, C.-Y., Ho Minh Le, T., & Park, D.-W. (2023). Full-scale investigation on inclined ballastless cant track using concrete slab panel at high temperature setting. *Construction and Building Materials*, *366*, 1–19.

Lee, S.-H., Choi, Y.-T., Lee, H.-M., & Park, D.-W. (2016). Performance evaluation of directly fastened asphalt track using a full-scale test. *Construction and Building Materials*, *113*, 404–414. https://doi.org/10.1016/j.conbuildmat.2016.02.221. Available from: < Go to ISI > ://WOS:000375817400041.

Lee, S.-H., Eum, K.-Y., Tri Ho Minh, L., & Park, D.-W. (2021). Evaluation on mechanical behavior of asphalt concrete trackbed with slab panel using full-scale static and dynamic load test. *Construction and Building Materials*, *276*, 1–20.

Lee, S.-H., Park, D.-W., Vo, H. V., & Fang, M. (2019). Analysis of asphalt concrete track based on service line test results. *Construction and Building Materials*, *203*, 558–566. https://doi.org/10.1016/j.conbuildmat.2019.01.131

Li, W., Jieling, X., Qiang, W., Ping, W., Guangsheng, L., & Xinwei, L. (2018). Reasonable track stiffness of embedded rail structure used in metro. *Journal of Central South University (Science and Technology)*, *149*(7), 1831–1837.

Li, J., Shang, M., Liu, G., Yang, T., Pan, Y., Zhou, J., & Zhao, Y. (2019a). Two-step improvements of volumetric design method based on multi-point supported skeleton for asphalt mixtures. *Construction and Building Materials*, *217*, 456–472. https://doi.org/10.1016/j.conbuildmat.2019.05.076

Li, J., Shang, M., Pan, Y., Liu, G., Chen, A., Zhou, J., & Zhao, Y. (2019b). Laboratory improvement and field assessment of volumetric design method based on multi-point supported skeleton for asphalt mixtures (v-s method). *Construction*

and Building Materials, *224*, 962–979. https://doi.org/10.1016/j.conbuildmat.2019.07.114. Available from: < Go to ISI > ://WOS:000487572800079.

Lira, B., Jelagin, D., & Birgisson, B. (2013). Gradation-based framework for asphalt mixture. *Materials and Structures*, *46*(8), 1401–1414. https://doi.org/10.1617/s11527-012-9982-3. Available from: < Go to ISI > ://WOS:000322493800015.

Liu, S., Chen, X., Ma, Y., Yang, J., Cai, D., & Yang, G. (2019). Modelling and in-situ measurement of dynamic behavior of asphalt supporting layer in slab track system. *Construction and Building Materials*, *228*, 1–15.

Liu, G., Qian, Z., Yang, D., Chen, L., Chua, D. K. H., & Li, Z. (2024). Dynamic behaviour of asphalt concrete substructure ballastless track system in long-span railway bridge. *Road Materials and Pavement Design*, *25*(1), 204–218. https://doi.org/10.1080/14680629.2023.2199881

Liu, Y., Qian, Z.-D., Zheng, D., & Huang, Q.-B. (2018). Evaluation of epoxy asphalt-based concrete substructure for high-speed railway ballastless track. *Construction and Building Materials*, *162*, 229–238. https://doi.org/10.1016/j.conbuildmat.2017.12.028. Available from: < Go to ISI > ://WOS:000425564400023.

Luo, R., Liu, H., & Zhang, Y. (2016). Characterization of linear viscoelastic, nonlinear viscoelastic and damage stages of asphalt mixtures. *Construction and Building Materials*, *125*, 72–80. https://doi.org/10.1016/j.conbuildmat.2016.08.039

Prowell, B. D., Brown, E. R., Anderson, R. M., Shen, S., Carpenter, S. H., & Aapt, Y. (2010). Endurance limit of hot mix asphalt mixtures to prevent bottom-up fatigue crackinged. ∧eds. 85th Association-of-Asphalt-Paving-Technologists Annual Meeting and Technical Sessions, Sacramento, CA, pp. 519–560.

Ramirez Cardona, D., Di Benedetto, H., Sauzeat, C., Calon, N., & Rose, J. G. (2020). Designs, application and performances of asphalt/bituminous trackbeds in European, Asian, and African countries. *Transportation Research Record: Journal of the Transportation Research Board*, *2674*(11), 245–262. https://doi.org/10.1177/0361198120945314. Available from: < Go to ISI > ://WOS:000566171800001.

Selig, E. T., & Li, D. (1994). Track modulus: Its meaning and factors influencing it.

Shan, Y., Cheng, G., Gu, X., Zhou, S., & Xiao, F. (2021). Optimization of design parameters of displacement isolation piles constructed between a high-speed railway bridge and a double-line metro tunnel: From the view point of vibration isolation effect. *Computers and Geotechnics*, *140*, 1–16.

Shi, C., Sun, X., Wang, T., Wu, Y., Liu, S., Wang, H., Yang, J., Xu, Y., & Qie, L. (2022). Numerical analysis of dynamic behavior of bi-block precast asphalt trackbed for high-speed railway. *Construction and Building Materials*, *342*, 1–12.

Shi, C., Zhang, H., Wang, T., Zhou, Y., Liu, S., Wang, H., Yang, J., Xu, Y., & Qie, L. (2021). Design and performance evaluation of bi-block precast rubberized epoxy asphalt trackbed for railway. *Construction and Building Materials*, *313*, 1–11.

Soto, F. M. (2018). *Characterization of rubberized asphalt for railway sub-ballast. Improvements in the mix-design, performance features and rational methodology of hma_rumac blends for railways*. Lambert Academic Publishing.

Soto, F., & Mino, G. (2018). Improvements in the mix-design, performance features and rational methodology of rubber modified binders for the thermal evaluation of the railway sub-ballast. *International Journal of Research Science & Management*, *5*(2), 1–22.

Tong, Y., Liu, G., Yousefian, K., & Jing, G. (2022). Track vertical stiffness -value, measurement methods, effective parameters and challenges: A review. *Transportation Geotechnics*, *37*, 1–12.

Tucho, A., Indraratna, B., & Ngo, T. (2022). Stress-deformation analysis of rail substructure under moving wheel load. *Transportation Geotechnics*, *36*, 1–19. https://doi.org/10.1016/j.trgeo.2022.100805

Wang, T., Shi, C., Yu, Y., Xu, G., Liu, S., Wang, H., Yang, J., Gong, M., Xu, Y., & Qie, L. (2022). Mechanical properties evaluation of crumb rubber asphalt mixture for elastic trackbed. *Construction and Building Materials*, *331*, 1–11.

Wu, Y., Shi, C., Yu, Y., Chen, H., Fan, Y., Wang, H., Yang, J., & Huang, W. (2023). Dynamic behavior of precast epoxy asphalt track bed for transition zone in high-speed railway: A numerical approach. *Transportation Geotechnics*, *40*, 1–14.

Xing, L. (2021). *Experimental and numerical investigations for macro- and meso-mechanical properties of glued ballast bed in high-speed railway*. Beijing Jiaotong University.

Yu, J., Chen, F., Deng, W., Ma, Y., & Yu, H. (2020). Design and performance of high-toughness ultra-thin friction course in south china. *Construction and Building Materials*, *246*, 1–12.

Zhang, Y., Cheng, H., Sun, L., Liu, L., & Hu, Y. (2021). Determination of volumetric criteria for designing hard asphalt mixture. *Construction and Building Materials*, *278*, 1–12.

Zhang, Y., Luo, X., Onifade, I., Huang, X., Lytton, R. L., & Birgisson, B. (2019). Mechanical evaluation of aggregate gradation to characterize load carrying capacity and rutting resistance of asphalt mixtures. *Construction and Building Materials*, *205*, 499–510. https://doi.org/10.1016/j.conbuildmat.2019.01.218. Available from: https://www.sciencedirect.com/science/article/pii/S0950061819302508

Zhang, D., Muhammad Sani, B., Xu, P., Liu, K., & Gu, F. (2023). Preparation and characterization of binary eutectic phase change material laden with thermal conductivity enhancer for cooling steel slag asphalt pavement. *Construction and Building Materials*, *388*, 1–14.

Zheng, C., Zhao, D., Xiang, N., & Song, Z. (2012). Mechanism of low-temperature adhesion failure in asphalt mixtures with dense-suspension and void-skeleton structures. *Construction and Building Materials*, *36*, 711–718. https://doi.org/10.1016/j.conbuildmat.2012.06.058. Available from: https://www.scopus.com/inward/record.uri?eid = 2-s2.0-84863832119&doi = 10.1016%2fj.conbuildmat.2012.06.058&partnerID = 40&md5 = 74ad2fc7dd00666b71e101fa2b27a3d3

Zhou, J., Chen, X., Fu, Q., Xu, G., & Cai, D. (2019). Dynamic responses of asphalt concrete waterproofing layer in ballastless track. *Applied Sciences-Basel*, *9*(3), 1–19.